Correlation between composition, microstructure, and emission properties in Nd-doped Si-rich Si oxynitride films: investigation into the nature of the sensitizer

C-H Liang, Y-T An, W Jin, D-C Meng, W. Wang, C-A Chen, K-Z Liu, W Kleyn, C. Labbe, Julien Cardin, et al.

Correlation between composition, microstructure, and emission properties in Nd-doped Si-rich Si oxynitride films: investigation into the nature of the sensitizer

C-H Liang[1], Y-T An[1], W Jin[1], D-C Meng[2], D-P Wang[1], C-A Chen[1], K-Z Liu[1], A W Kleyn[1], C Labbé[3], J Cardin[3] and F Gourbilleau[3]

[1] Institute of Materials, China Academy of Engineering Physics, 610200 Chengdu, Sichuan, People's Republic of China
[2] Microsystem and Terahertz Research Center & Institute of Electronic Engineering, China Academy of Engineering Physics, 621900 Mianyang, People's Republic of China
[3] CIMAP, Normandie Univ., ENSICAEN, UNICAEN, CEA, CNRS, 6 Boulevard Maréchal Juin F-14050 Caen Cedex 4, France

E-mail: anyt03@163.com

Received 25 July 2018, revised 15 October 2018
Accepted for publication 22 October 2018
Published 21 November 2018

Abstract

Rare earth (*RE*) ions doped in Si-based materials, compatible with Si technology, are promising compounds with regards to optical communication and energy conversion. In this article, we show the emission properties of Nd-doped Si-rich Si oxynitride (Nd-*SRSON*) films, and their dependence on the dangling bond density and the nature of the sensitizer. These films were prepared by reactive magnetron sputtering and post-annealing. The film composition, microstructure, and emission properties were investigated as a function of deposition parameters and annealing temperatures. Both Fourier transform infrared (*FTIR*) and ellipsometry spectroscopy measurements have confirmed that the sample composition (Si/N ratio) can be carefully tuned by varying the ratio of reactive nitrogen to argon in the sputtering plasma. Moreover, *FTIR* and x-ray photoelectron spectroscopy measurements demonstrate the existence of both nitrogen and oxygen dangling bonds ($N^{\cdot}$ and $O^{\cdot}$) in as-deposited samples. These dangling bonds were passivated during annealing. Under non-resonant excitation at 488 nm, the films exhibit a significant photoluminescence (*PL*) signal from Nd^{3+} ions demonstrating the occurrence of an effective sensitization of Nd^{3+} ions in the host matrix. Both *PL* excitation and ellipsometry results (the energy band gap from new amorphous model) exclude the sensitization by an exciton with energy over the band gap, whereas the presence of Si agglomerates, at the atomic scale, have been identified as effective sensitizers towards Nd^{3+} ions. This work not only provides knowledge to optimize Si-based materials for favorable emission properties, but also, presents a universal methodology to investigate the nature of sensitizers for *RE* emitters. This allows one to find correlations between composition, microstructure, and emission properties.

Keywords: neodymium, rare earth, Si-rich Si oxynitride, thin film, non-resonant excitation, photoluminescence

Introduction

Silicon photonics has attracted considerable attention since it has a potential application in microelectronics and more recently in silicon-based materials for energy conversion [1–3]. For this reason, systems composed of rare earth (*RE*) ions incorporated in silicon-based host matrices have been intensively investigated [4–8]. In such systems, the presence of sensitizers such as silicon nanoparticles (Si–nps) can allow an increase of the effective excitation cross section of *RE* ions by several orders of magnitude [9, 10]. However, an effective sensitization process is governed by energy transfer (*ET*) mechanism that is strongly distance dependent. This *ET* is either a Coulombic type (Förster) or carrier exchange based (Dexter), with an interaction distance ranging from some nanometers for Förster-approach [11] to below a nanometer for Dexter-interaction [12]. A large distance between the sensitizer and the *RE* ion, as well as the clustering of *RE* ions (formation of RE_2O_3 for example) in the Si-based host matrix are considered as two major factors that could limit the coupling of *RE* ions with the sensitizer. This situation requires, therefore, some nano-engineering of the material composition (i) through growing a high density of sensitizers in order to enhance the *RE*-related emission, (ii) by increasing the concentration of *RE* ions before the concentration quenching effect becomes dominant [7].

The Er-doped Si-rich Si oxide (Er-*SRSO*) system has been widely studied. Early results stated that the *ET* between Si–nps and Er^{3+} ions is optimal for crystallized Si–nps [13], but amorphous Si–nps were later shown to play an efficient sensitizing role towards the Er ions as well [14, 15], demonstrating that crystallization is not a prerequisite. From such results, it was found that crystallized Si–nps appear in general at high temperature 1100 °C, and the amorphous one at about 900 °C or below. This former would favor a coalescence of Si–nps as well as the formation of Er_2O_3, which consequently decrease the number of sensitizers, and increase the distance between them and the Er^{3+} ions. The consequence is an observed quenching of the *RE* emission [16]. At low annealing temperature (<900 °C), our previous work has evidenced the presence of Si-based sensitizers issue from the agglomeration of less than 15 Si atoms [16]. This allows to obtain a high density of sensitizers uniformly distributed leading thus to a high fraction (22%) of optically active Er^{3+} ions effectively coupled to sensitizers [17]. Up to now, the achievement of net gain from such an Er-*SRSO* system is, however, rather rare or even shown as impossible [18, 19].

An alternative system, Nd-doped Si-rich Si nitride (Nd-*SRSN*), attracts strong interest in recent years. In contrast to the three-level electronic 4f structure for the Er^{3+} ion, in the case of the Nd^{3+} ion it is easier to achieve net gain due to its four-level configuration considering the $^4F_{3/2} \rightarrow {}^4I_{11/2}$ transition leading to a 1.06 μm emission. Our simulation work has demonstrated that a significant positive net gain up to 30 dB cm^{-1} can be achieved with the Nd-doped *SRSO* waveguide [19]. For the host matrix, the *SRSN* matrix has a much higher threshold for *RE* ions agglomeration than the oxide case. This may be due to low diffusion coefficients for *RE* ions in a nitride matrix [20, 21]. This means that more optically active *RE* ions may potentially be present in *SRSN* than in *SRSO* matrices. Moreover, Li *et al* have observed a maximum Nd^{3+} photoluminescence (*PL*) intensity corresponding to a Si concentration of 45% [22]. These authors proposed that localized states present in high density in the band-tails act as effective sensitizers to Nd^{3+} ions for such oxygen-free Nd-*SRSN* sample. Marcus *et al* have observed that *RE* ions tend to be surrounded by oxygen atoms, an arrangement considered as crucial for the optical activation of *RE* ions in glasses, and particularly for efficient emission [23, 24]. This statement implies the importance to carefully incorporate a small amount of oxygen in the host matrix. However, the work on Nd-doped Si-rich Si oxynitride (Nd-*SRSON*) system is quite scarce. The sensitizer nature requires a deeper analysis to see whether there is a difference comparing to other Si-based systems.

In our previous work on Tb-doped N-rich Si oxynitride (Tb-*NRSON*), we have confirmed that both band-tails and N_4^+ defect states can play the role of sensitizers towards Tb^{3+} ions [3]. Herein, we propose to study a different system, Nd-*SRSON* sample. It consists of an Nd-doped oxynitride Si-based matrix in which we have incorporated a Si excess. This study aims at (i) optimizing the Nd^{3+} emission through variation of deposition parameters for tuning the sample composition and annealing conditions for controlling the sample microstructure, and (ii) elucidating the Nd^{3+} ions excitation mechanisms correlated with composition and microstructure. This work has not only to do with waveguide applications in the case of Nd^{3+} ions, but also with the *RE*-doped Si-based systems as frequency conversion layers, see for example [21, 25, 26].

Experiment

The films of about 400 nm thick were deposited by radio frequency magnetron co-sputtering of two confocal cathodes (Si and Nd_2O_3) driven by plasma constituting of a mixture of nitrogen and argon. The p-type mono-crystalline Si or fused silica substrates were used and maintained at 200 °C during the growth. Films deposited on fused silica as substrate were developed only for Raman measurements, other experiments were carried out on films grown on Si substrate. The plasma power densities for Si and Nd_2O_3 targets were fixed at 4.44 and 0.44 W cm^{-2}, respectively. The ratio of N_2 to Ar gas flux (r_N) was varied from 7.0% to 13.3%, while the gas pressure of the plasma was kept constant at 2 mTorr. Such deposition parameters allow one to incorporate a Si excess in the films. Thus, these later are named as Nd-*SRSON*, which will be confirmed below by the characterizations of their composition. After deposition, the films were submitted to a thermal annealing treatment under N_2 ambient for 1 min durations, and different temperatures ranging from 600 °C to 1100 °C. The chemical composition, microstructure, and optical properties of as-deposited and annealed films were studied by x-ray photoelectron spectroscopy (XPS), Fourier transform infrared (*FTIR*), Raman, ellipsometry, transmission electron

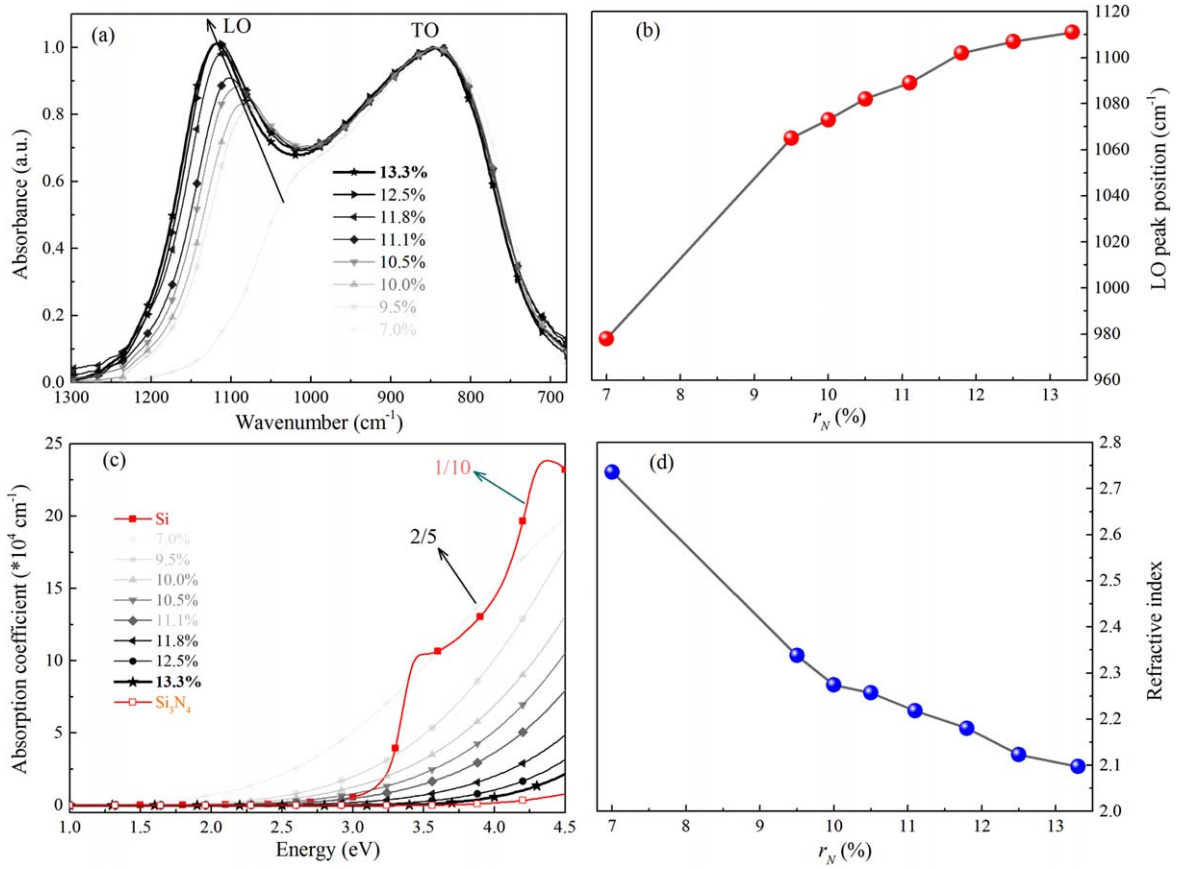

Figure 1. (a) *FTIR* spectra recorded with an incidence angle of 65° for different r_N values, (b) the position of *LO* peak obtained by fitting the *FTIR* spectra as a function of r_N, (c) absorption coefficient versus energy, and (d) refractive index given at 1.95 eV versus r_N for as-deposited layers. In (c) absorption coefficients of pure amorphous Si_3N_4 and Si are added for comparison purpose. The absorption coefficients for pure Si and $r_N = 7.0\%$ are multiplied by $1/10$ and $2/5$, respectively.

microscopy (*TEM*), *PL* and photoluminescence in excitation (*PLE*) spectroscopies.

The *XPS* measurements were performed in an ultra-high vacuum *PHI*-5000 *VPII* system with a base pressure lower than 5×10^{-8} Pa using a mono-chromatic Mg $k\alpha$ radiation at 1253.6 eV. The layer surface was cleaned (sputtered) by 2 keV Ar^+ bombardment for 2 min before the measurements. The binding energy was calibrated by using the value of contaminant carbon C1s = 284.8 eV as reference. For *FTIR* measurements, the spectra were recorded at 65° incidence angle in the 500–4000 cm^{-1} range using a Nicolet Nexus 470 spectrometer. In case of Raman characterization, the incident laser wavelength was 532 nm. The ellipsometry experiments were carried out by means of an *UVISEL* Jobin–Yvon ellipsometer with an incident angle of 66.2°. The experimental spectra were recorded on a 1.5–5 eV range with 0.01 eV resolution. The absorption coefficient, refractive index, and thickness were deduced from the experimental data by fitting with the new amorphous dispersion formula which is derived from the Forouhi–Bloomer model for amorphous semiconductors using the *DeltaPsi2* software [27]. The model takes into account the use of crystalline Si substrate, an amorphous Si oxynitride, a rough surface layer composed of a mixture of void space and Si oxynitride. The *TEM* measurements were performed in bright and dark field modes on a cross-sectional sample using a JEOL 2010F (200 kV) microscope. The *PL* experiments were carried out using the 488 nm-line of a *CW* Argon laser (*Innova* 90 *C Coherent*), which is a non-resonant wavelength for Nd^{3+} ions [28]. Finally, the *PLE* spectra were collected by means of Jobin–Yvon Fluorolog spectrophotometer using a Xe lamp as excitation source. The *PLE* spectra shown below have been calibrated to the spectrum of the Xe lamp used.

Results and discussion

Effect of composition

As nondestructive techniques, both *FTIR* spectroscopy and spectroscopic ellipsometry were adopted to study the microstructural and optical properties of dielectric films. Figure 1(a) shows the evolution of the *FTIR* spectra recorded for as-deposited films prepared with the indicative r_N. Two main vibrations bands are clearly visible, peaking at about 830 cm^{-1} and between 970 and 1150 cm^{-1}. They correspond to the transverse and longitudinal optical (*TO* and *LO*) vibrations bands from Si–N bond, respectively. All spectra are normalized to the intensity of TO_{Si-N} band. The TO_{Si-N} band position slightly changes with r_N, whereas the

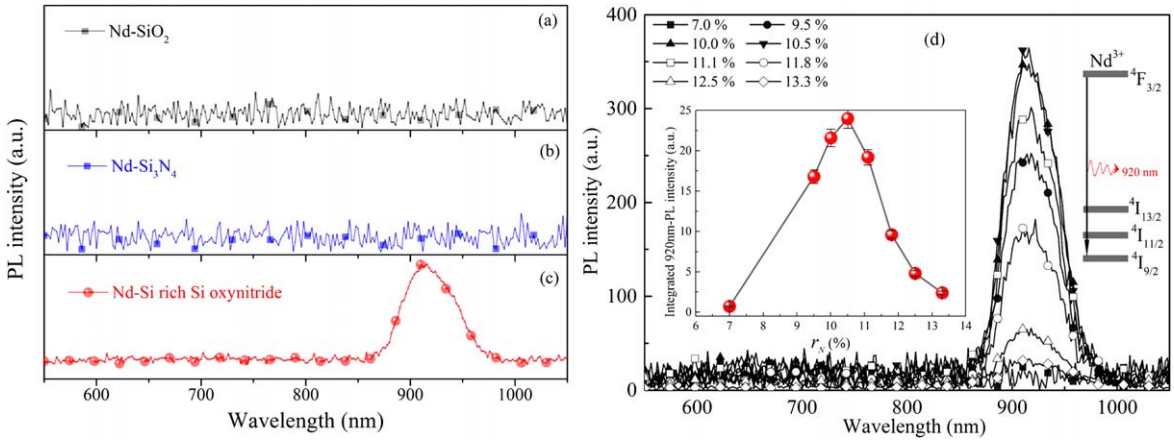

Figure 2. *PL* spectra for Nd-doped in the indicative matrix (a) SiO_2, (b) Si_3N_4, (c) *SRSON* prepared with $r_N = 10.5\%$, and (d) Si-rich Si oxynitride with different r_N ranging from 7.0% to 13.3%; in (d) the inset shows the integrated 920 nm peak intensity versus r_N and the right depicts the origin of 920 nm peak from $^4F_{3/2}$–$^4I_{9/2}$ transition in the Nd^{3+} ions.

evolutions of $LO_{Si–N}$ position and intensity are more pronounced. The $LO_{Si–N}$ peak position, obtained by fitting with Gaussian formula, is displayed in figure 1(b). Thus, a significant blue-shift of $LO_{Si–N}$ peak position and a concomitant increase of its intensity with r_N can be noticed. Such behavior is ascribed to a remarkable increase of Si–N bonds and thus confirms an enhancement of N content in the host matrix [29]. As presented in figure 1(c), each value of the absorption coefficient is lower than $10^3\ cm^{-1}$ in the 1.0–1.5 eV range. For higher energies from 1.5 to 4.5 eV, it can reach some tens of $10^4\ cm^{-1}$. As noticed, all these curves are between those of amorphous Si_3N_4 and Si materials. The absorption coefficient curve for the sample with $r_N = 13.3\%$ is close to that of amorphous Si_3N_4, while with decreasing r_N the absorption coefficient increases towards the value of amorphous Si. Moreover, the refractive index shown in figure 1(d) decreases with r_N which demonstrates that the increase of the nitrogen content in the plasma diminishes the Si incorporation in the Si3N4 matrix. This evolution is in agreement with the *FTIR* results confirming that r_N is an effective parameter to carefully tune the layer composition, i.e. the Si/N ratio.

Figures 2(a)–(c) present the *PL* spectra for Nd-doped in stoichiometric SiO_2, Si_3N_4, and *SRSON* matrices. No *PL* signal was observed from the former two matrices, while the latter exhibits a remarkable peak at about 920 nm. This suggests an excess of Si in the matrix is required to achieve *PL* signal. Thereafter, the *PL* spectra dependence on nitrogen rate r_N used to prepare the samples are shown in figure 2(d). To note that, all these spectra come from the samples with annealing at 750 °C, which corresponds to an optimal temperature as described below. No emission is seen from 500 to 800 nm for any r_N value. However, one can clearly observe a *PL* peak centered at 920 nm ascribed to the $^4F_{3/2}$–$^4I_{9/2}$ transition in the Nd^{3+} ions [30]. Such an emission achieved with a non-resonant excitation wavelength (488 nm) for the Nd^{3+} ions confirms the presence of sensitizers towards this *RE* ions in the host matrix. The integrated *PL* intensity of Nd^{3+} (inset of figure 2(d)) gradually increases with the r_N increases from 7.0% to 10.5%, then falls down for higher r_N values (from 11.1 to 13.3%). The Nd content is assumed to remain constant since the applied power density on the Nd_2O_3 cathode was the same for all these samples. Thus, the evolution of Nd^{3+} *PL* intensity is probably determined by the Si/*N* ratio. As estimated by *XPS* measurements, the optimized sample (for $r_N = 10.5\%$) was found to contain 47.4, 46.2, 5.7, 0.8 at% for Si, N, O, Nd element, respectively. The Si concentration is excessive comparing to those in Si_3N_4 and SiO_2, thus the sample is called Nd-doped Si-rich Si oxynitride (Nd-*SRSON*).

Effect of microstructure

To further understand the *PL* dependence, it is important to investigate the effect of microstructure influenced by thermal annealing conditions. The optimized layer ($r_N = 10.5\%$) has been studied by *FTIR* and Raman spectroscopes, *TEM* and *XPS* experiments. Figure 3(a) shows the layer microstructure evolution for different annealing temperatures ranging from 600 °C to 1100 °C using *FTIR* experiments. All spectra are normalized to the $TO_{Si–N}$ band intensity. In contrast to the as-deposited sample, the $LO_{Si–N}$ peak intensity increases and shifts towards higher wavenumbers for annealed samples. For the former, such a behavior means that the number of Si–N bonds increases due to annealing. This implies the presence of some N dangling bonds in the as-deposited matrix, which recombine with Si atoms upon annealing. Moreover, the $LO_{Si–N}$ peak intensity approaches near saturation after annealing at 600 °C. This suggests that an achievement of the recombination of N· dangling bonds with Si to form Si–N bond does not require higher temperatures such as 1100 °C. By the way, the intensity of $LO_{Si–N}$–$TO_{Si–N}$ bands overlapping at about $1010\ cm^{-1}$ is gradually attenuated with increasing temperature. This behavior suggests that the host matrix becomes more ordered by the atomic rearrangement. The peak centered at $1250\ cm^{-1}$ is attributed to a Si–O bond. Such a peak appears after annealing and its intensity increases with temperature. This is probably due to a phase separation within the matrix induced by the thermal treatment.

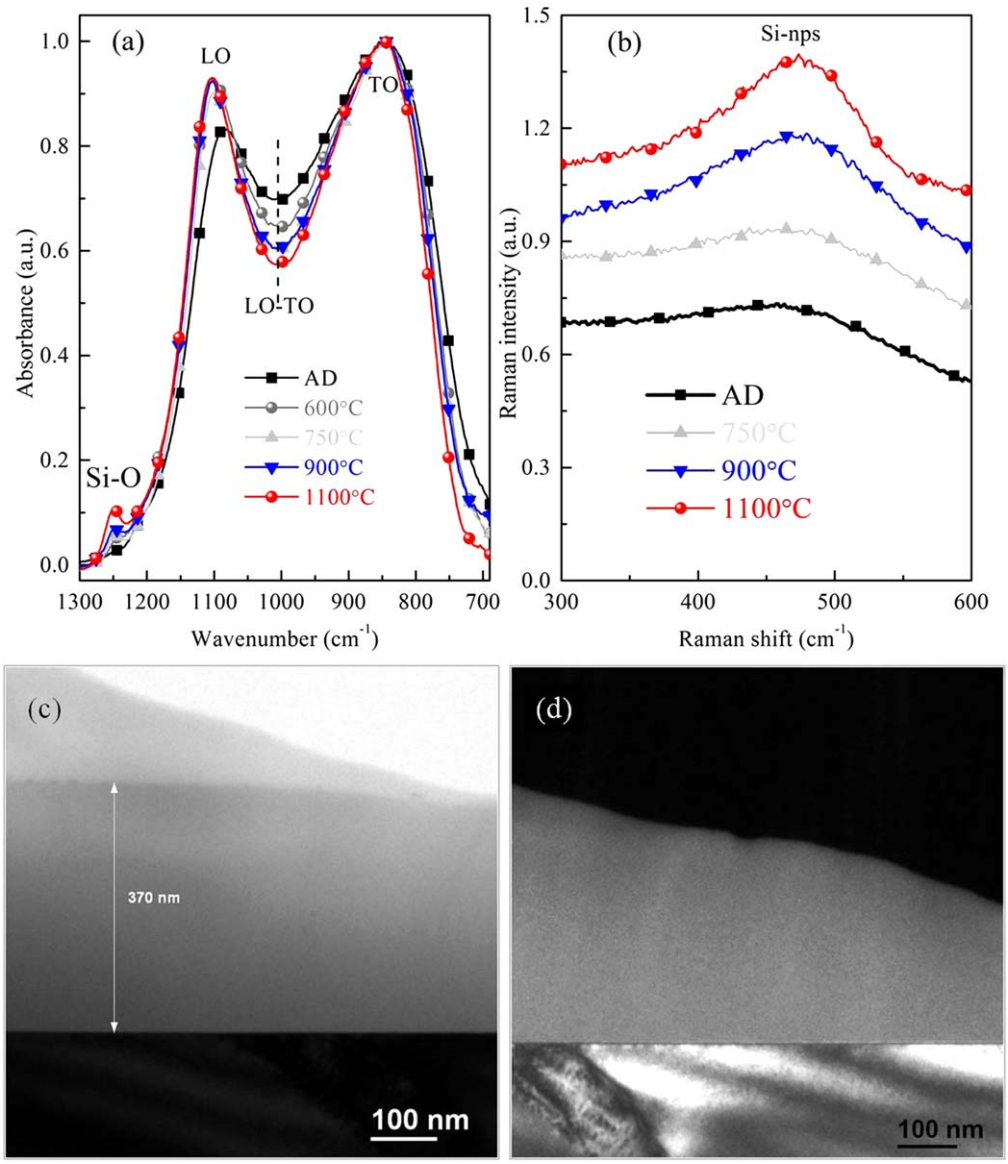

Figure 3. (a) *FTIR* spectra recorded with an incidence angle of 65° and (b) Raman spectra for the optimal Nd-*SRSON* layer as-deposited (*AD*) and annealed at the indicated temperatures, *TEM* pictures for 1100 °C-annealed film taken in bright (c) and dark (d) field modes.

Figure 3(b) reports the Raman experiments performed on corresponding as-deposited, 750 °C-, 900 °C- and 1100 °C-annealed samples. Both as-deposited and 750 °C-annealed samples present a weak band at about 480 cm^{-1}. This suggests that the Si–nps density is very low for these two thin films. With T_A increase especially at 1100 °C, the spectra show a remarkable peak. It attests the increase of amorphous Si–nps number within the host matrix [31]. It also confirms a structural rearrangement of the matrix and/or a phase separation in the Nd-*SRSON* materials under such a high annealing temperature. The absence of a peak at about 521 cm^{-1} indicates that no crystalline Si–nps have been formed upon 1100 °C-annealing temperature process. The *TEM* results are shown in figures 3(c) and (d). The observations exclude the presence of crystal in the film annealed at 1100 °C. This agrees well with the Raman experiments and strongly confirms that the Si atoms assemble during annealing as amorphous species.

The *XPS* spectra can provide the chemical surrounding, i.e. atomic binding condition in the samples. For the Si element, according to the random bonding model, each Si atom coordinates to four atoms in the *SRSON* matrix and forms tetrahedral units Si–$Si_kN_xO_y$ ($k + x + y = 4$; k, x, $y = 0$, 1, 2, 3, 4). Figure 4 shows the Si 2*p* *XPS* spectra and components peaks for the optimal sample as-deposited (figure 4(b)) and annealed at the indicated temperature (figures 4(c), (d)). The Si 2*p* *XPS* spectrum of Si wafer used as substrate is also added for comparison (figure 4(a)). Four component peaks were obtained after a de-convolution process. Two peaks centered at 103.8 and 99.2 eV have been experimentally observed and respectively attributed to Si–O_4 and Si–Si_4 species [32–34]. For the former, the peak intensity is quite low for the as-deposited layer and shows an enhancement upon annealing. This suggests the O atoms in as-deposited layers are located in a metastable state, rearrange locally and thus form Si–O bonds during annealing. For the later, the

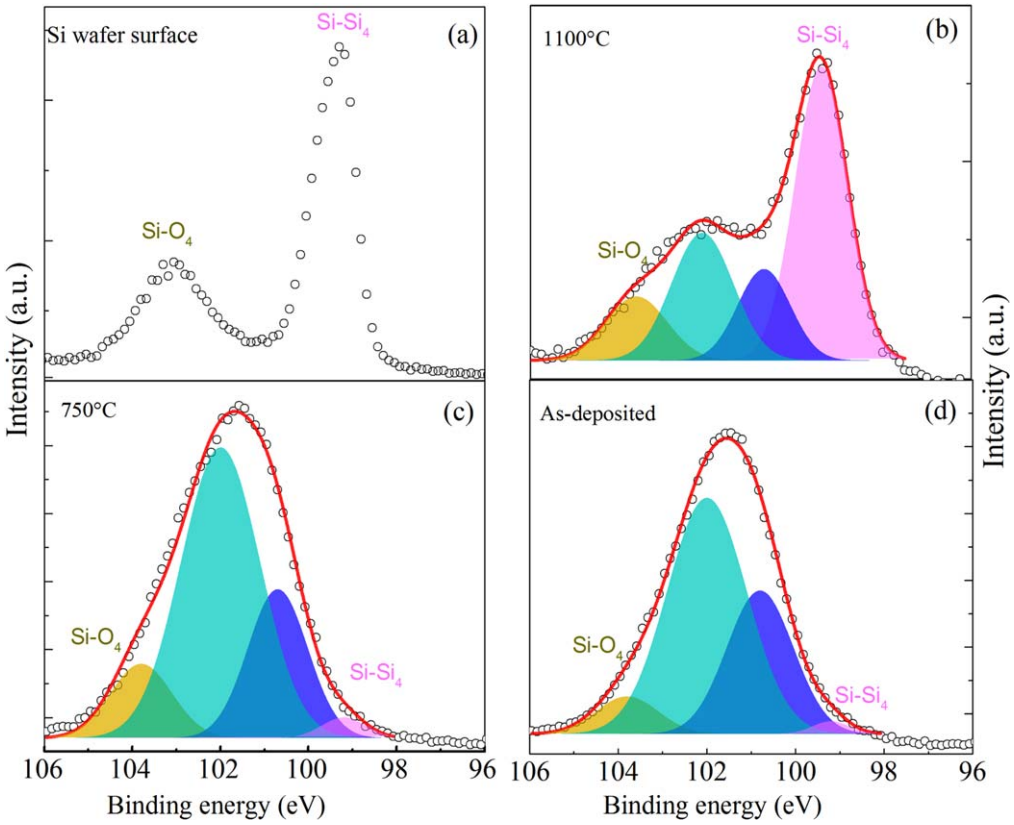

Figure 4. The raw Si $2p3/2$ spectra data (open circles) and component peaks (filled area) obtained from the fit of the high-resolution *XPS* spectra in the Si $2p3/2$ region for the optimized sample (for $r_N = 10.5\%$) annealed at the indicated temperature ((b–d)) and Si wafer (a).

peak intensity is rather low for the as-deposited film. It is slightly enhanced by annealing at 750 °C, while it significantly increases at 1100 °C. This agrees well with Raman results and again evidences that a phase separation occurred after high temperature annealing. In case of the other two components peaking at 101.9 and 100.8 eV, they are assigned to the tetrahedrons containing Si–Si bonds, i.e. k'=1, 2, or 3 in Si–$Si_{k'}N_xO_y$ formula ($k' + x + y = 4$; x, $y = 0$, 1, 2, 3) according to the calculation by Cova *et al* [35]. In comparison with the case of $k = 0$, such Si–$Si_{k'}N_xO_y$ species are named in this paper as Si-rich tetrahedrons. The tetrahedron corresponded to 100.8 eV has a higher k' value than that for 101.9 eV. As noticed, these two components from Si-rich tetrahedrons mainly occupy the Si $2p$ peak area for the as-deposited sample. Their intensities relative to Si–Si_4 species show a little decrease after a 750 °C annealing treatment and a remarkable decrease at 1100 °C one. For this later case it indicates the decomposition of Si-rich tetrahedrons and thus the formation of Si–Si_4 species.

In case of N 1 *s* binding energy region (figure 5(a)), the peak centered at 397.8 eV is observed for the as-deposited sample and presents a red shift for annealed ones. This shift means that the N oxidation state decreases after annealing [36, 37]. Since the oxidation state is dependent on the coordination number in the system, which mainly contains N and Si atoms, one would thus infer the existence of an N-SiN_x ($x < 3$) species with dangling bonds in the as-deposited sample. During annealing, the N-SiN_x ($x < 3$) species converts to an N-Si_3 leading to a passivation of the N· dangling bond [38]. In case of O 1 *s* binding energy region (figure 5(b)), the peak locates at about 532.9 eV for the as-deposited sample and gradually shifts to lower binding energy upon annealing. Note that the 1100 °C-annealed sample shows a broader band that can be fitted into two components peaking at 532.5 and 530.7 eV. The shift of the former component from 532.9 to 532.5 eV is explained by the conversion from O·–Si species into O–Si_2 species [39, 40]. This leads to an enhancement of Si–O bond number with annealing temperature, which is consistent with *FTIR* results (figure 3). The other component at 530.7 eV is assigned to an O–Nd bond [41]. It indicates the change of Nd surroundings under high temperature annealing. As displayed in figure 5(c) for Nd 3*d5/2* binding energy region, the 1100 °C-annealed sample shows a higher energy peak in contrast to both as-deposited and 750 °C-annealed samples. This peak is attributed to Nd–O bond, while the shift is interpreted by the increase of Nd oxidation state [42]. Figure 5(d), as a conclusion for 5(a)–(c), schematically depicts the evolution of chemical surrounding for N, O, and Nd. It illustrates the passivation of dangling bond upon thermal annealing.

The *PL* spectra are displayed in figure 6 for as-deposited and annealed films. The Nd^{3+} emission was recorded and its intensity versus T_A is shown in the inset. In contrast to the as-deposited sample, the annealing treatment significantly enhances Nd^{3+} *PL* intensity even at low $T_A = 600$ °C. When increasing T_A, the *PL* intensity is improved by a factor of

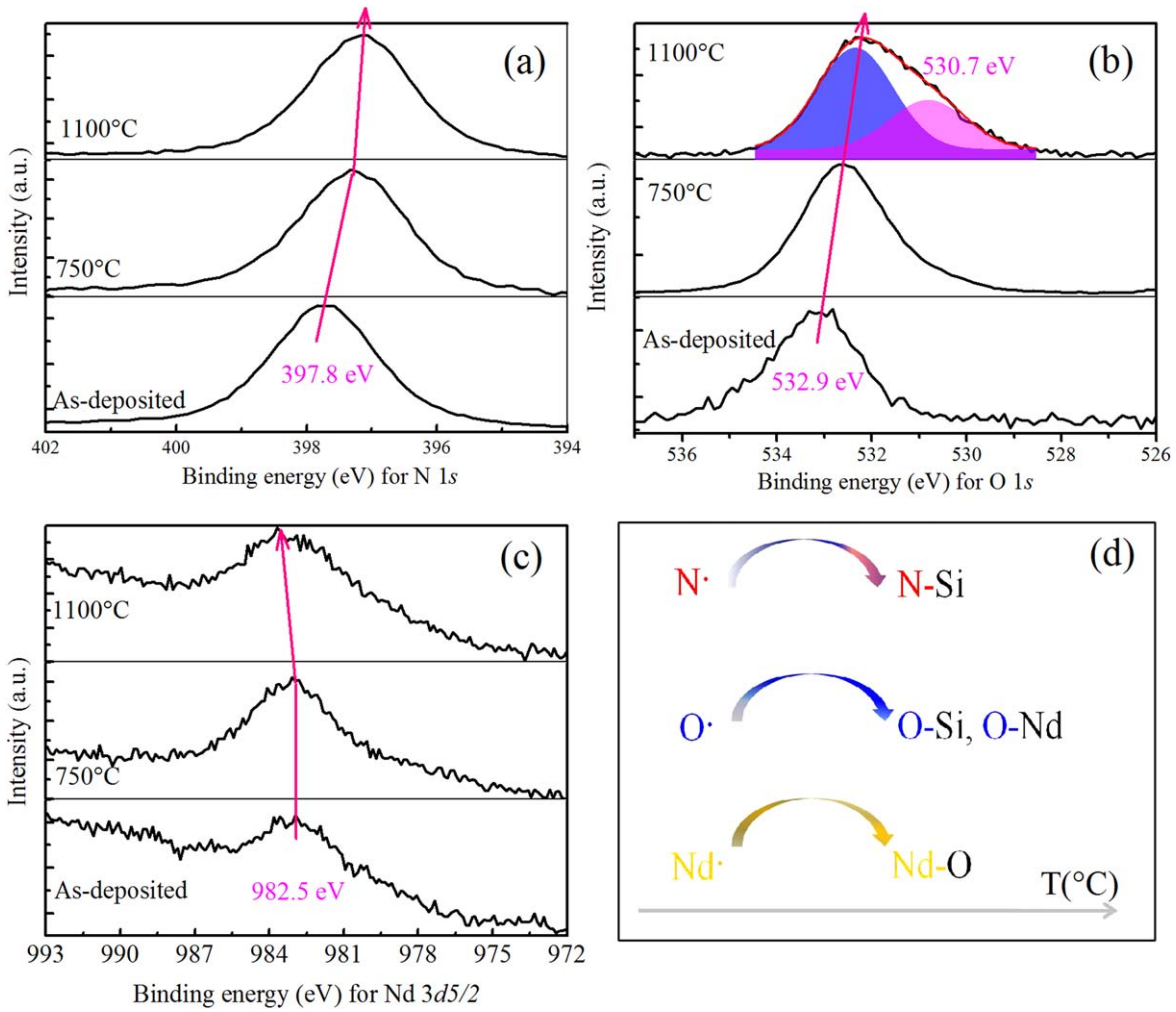

Figure 5. High-resolution *XPS* spectra for (a) N 1 *s*, (b) O 1 *s*, and (c) Nd 3*d5/2* binding energy region for the optimized sample ($r_N = 10.5\%$) annealed at the indicated temperature, (d) drawing of evolution of chemical surrounding for N, O, and Nd elements.

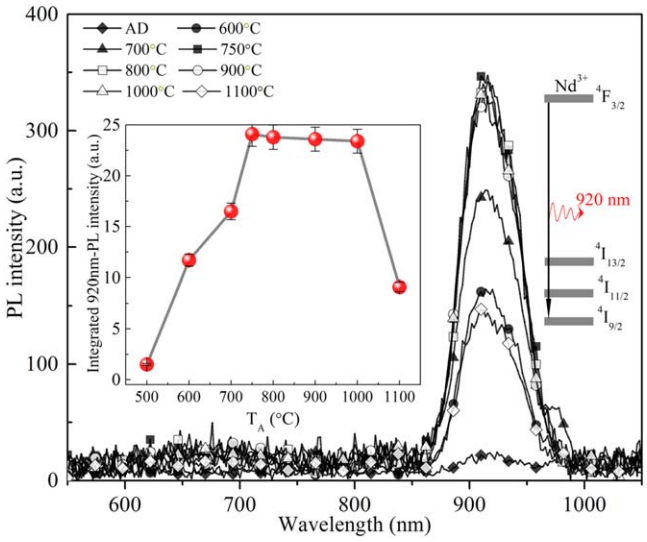

Figure 6. *PL* spectra of as-deposited (AD) and annealed samples (at indicated T_A, annealing temperature). The left inset shows the integrated *PL* intensity for 920 nm peak versus temperature and the right one depicts the origin of 920 nm peak from $^4F_{3/2}$-$^4I_{9/2}$ transition in the Nd^{3+} ions.

more than 10 before collapsing at 1100 °C. This behavior corresponds to the evolutions of matrix microstructure and chemical surrounding for Nd^{3+} ions, which determine the fraction of efficient coupling between sensitizers and Nd^{3+} ions. The samples show a high Nd^{3+} *PL* intensity in a quite wide range of moderate annealing temperatures ranging from 750 °C to 1000 °C. This is obtained by a concomitant effect of the recovering of non-radiative defects, the evolution of sensitizers' number and optically active Nd^{3+} density.

ET mechanisms

From ellipsometry data analyzed by means of new amorphous dispersion model, the energy band gap was estimated for various r_N in this study. The band gap energy, as shown in figure 7(a), varies from 2.1 to 4.6 eV with r_N varying from 7% to 13.3%. Such band gap enlargement is related to less Si incorporation in the Si_3N_4 matrix. This causes the matrix to become more ordered and the band-tails concomitantly shrink [43]. For $r_N = 10.5\%$ the band gap energy was found equal to about 4.0 eV, which is much higher than the excitation energy at 2.54 eV. Furthermore, *PL* excitation (*PLE*) measurement collected at 920 nm was carried out on the optimized sample

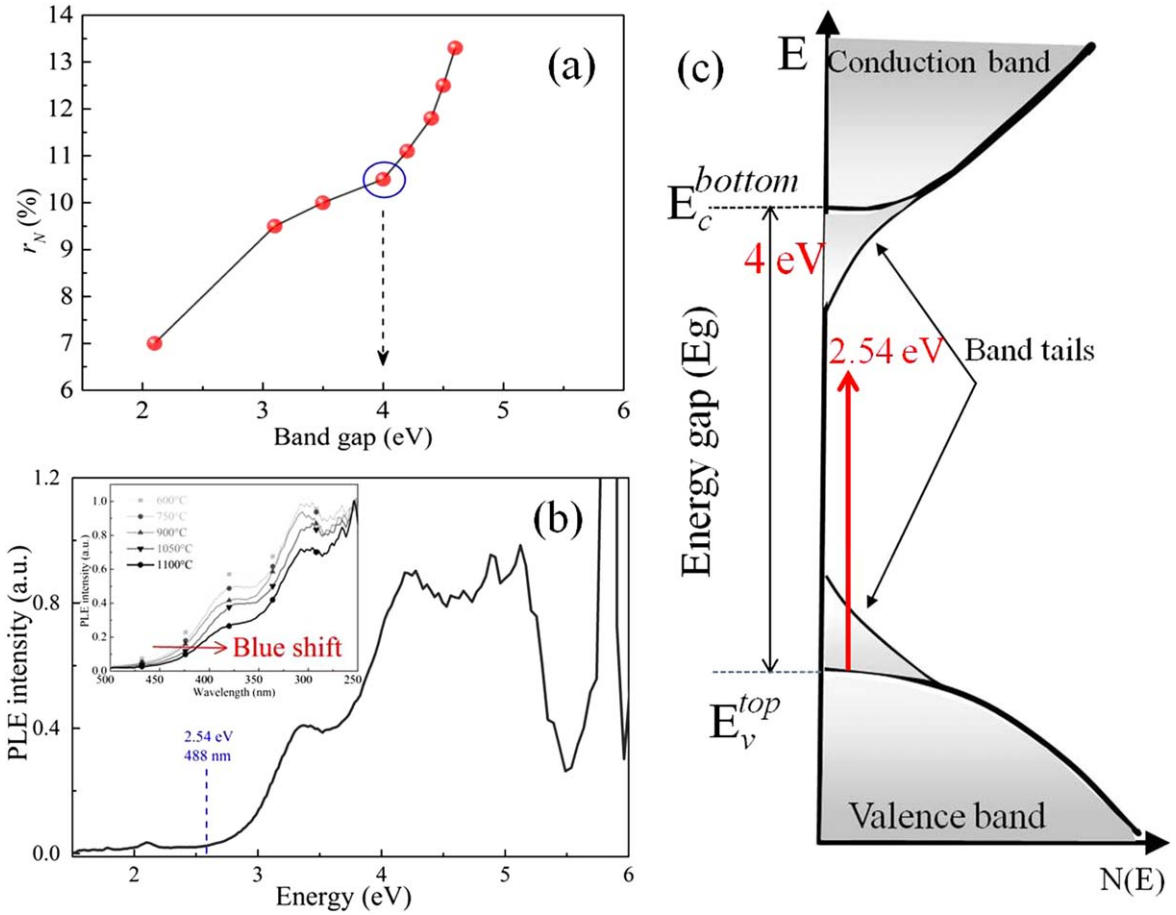

Figure 7. (a) r_N used to prepared samples versus band gap estimated by the new amorphous dispersion model, the 750 °C-annealed optimized samples ($r_N = 10.5\%$) corresponds to a band gap of 4.0 eV; (b) *PLE* spectra detected at 920 nm for optimized samples ($r_N = 10.5\%$) annealed at 750 °C. The inset shows the *PLE* spectra evolution for indicative values of T_A; (c) schematic illustration of the excitation photon with 2.54 eV compared to the matrix band gap and tails.

annealed at 750 °C and the obtained spectrum is shown in figure 7(b). As seen, the *PLE* intensity is weak for energy lower than 2.8 eV by comparison with the higher energy range (2.8–4.0 eV) where the *PLE* intensity increases with a slope shape. Such shape is a characteristic of band-tails to band-tails absorption mechanism in an amorphous silicon oxynitride matrix [25]. These spectra present a blue-shift with T_A increase. This shift is related to the passivation of defect density as well as to the shrinking of band-tails in the matrix. The matrix band gap and tails are schematically illustrated in figure 7(c). As seen, the excitation energy 2.54 eV used in this work does not reach the conduction band. Therefore, the sensitization of Nd^{3+} ions is not directly due to an *ET* occurring from exciton generated between conduction and valence band.

As discussed on figures 1 and 2, excessive Si in the matrix is required to form Si agglomerates and thus achieve Nd^{3+}-emission under a non-resonant excitation (488 nm) [44, 45]. These agglomerates, according to the *TEM*, Raman, and *XPS* experimental results, are amorphous and small for the optimized sample. This agrees well with our previous work demonstrating that a few Si atoms are enough to act as *RE* sensitizer [16]. Furthermore, the Si agglomerates at atomic scale, as observed by Salh *et al*, are optically active and display green–yellow emission [46]. The exciton emitting green–yellow light is likely to couple with the nearby Nd^{3+} ion [47]. Indeed, the visible emission was not observed in our case for the Nd^{3+} doped layers while a clear *PL* peak at 920 nm was present via a non-resonant wavelength excitation. This infrared *PL* at the expense of visible emission suggests the occurrence of efficient *ET* from atomic scale Si agglomerates to Nd^{3+} ions.

Following the discussion on the nature of the sensitizer, the correlation between the composition, microstructure, and emission properties are described here. Excess Si atoms are needed to create the atomic scale Si agglomerates. However, high Si/N ratio would result in a formation of large Si agglomerates. These latter are ineffective to transfer energy to Nd^{3+} ions [48]. Therefore, the Nd^{3+}-*PL* intensity shows a maximum value at a moderate Si/N ratio. Moreover, the non-radiative defects such as N and O should be recovered to achieve a high *PL* intensity. Annealing treatment shows a good approach to promote $N^{\cdot}$ and $O^{\cdot}$ recombination with Si, as evidenced by both *XPS* and *FTIR* results. Whereas, annealing at high temperature 1100 °C, too large Si agglomerates are grown by a decomposition of Si-rich tetrahedrons species. It would also result in the clustering of Nd ions, which favors an energy cross-relaxation process. This will

reduce the effective sensitizers and/or emitter centers. Such behaviors demonstrate the importance of controlling deposition parameter and annealing temperature to optimize sample composition and microstructure in order to (i) favor the generation of effective sensitizers, (ii) recover the non-radiative defects, (iii) promote the highest coupling number between sensitizers and lanthanide ions.

Conclusion

The correlation between the composition, microstructure, and emission properties of Nd-*SRSON* films have been studied in detail. The maximum *PL* intensity of Nd^{3+} ions was obtained from the films (i) deposited by reactive magnetron co-sputtering of pure Si and Nd_2O_3 cathodes under mixed ($N_2/Ar = 10.5\%$) plasmas, and (ii) post-annealed at 750°C–1000 °C. This, as demonstrated above, corresponds to the best environment for the achievement of dense effective sensitizers and for a passivation of non-radiative defects such as N· and O· dangling bonds. The optical measurements confirm that the excitation process of Nd^{3+} ions did not involve the valence-conduction band but the excitation rate is enhanced by atomic scale Si agglomerations. The overall analysis involves six types of optical measurements. This seems an effective methodology to monitor the evolution of composition and microstructure, such as Si agglomerations and non-radiative defects. This approach exhibits a great advantage to study atomic sensitizers towards *RE* ions and thus achieve favorable emission.

Acknowledgments

This work was financially supported by the Natural Science Foundation of China (Grant Nos. 11504343 and 51701194) and the French National Research Agency (Grant No. ANR-08-NANO-005).

ORCID iDs

Y-T An https://orcid.org/0000-0003-3280-9579

References

[1] Kenyon A J, Trwoga P F, Federighi M and Pitt C W 1994 *J. Phys.: Condens. Matter* **6** L319
[2] Franzo G, Pacifici D, Vinciguerra V, Priolo F and Iacona F 2000 *Appl. Phys. Lett.* **76** 2167
[3] Labbé C, An Y T, Zatryb G, Portier X, Podhorodecki A, Marie P, Frilay C, Cardin J and Gourbilleau F 2017 *Nanotechnology* **28** 115710
[4] Kik P G, Brongersma M L and Polman A 2000 *Appl. Phys. Lett.* **76** 2325
[5] Zatryb G, Klak M M, Wojcik J, Misiewicz J, Mascher P and Podhorodecki A 2015 *J. Appl. Phys.* **118** 243104
[6] Zanatta A R 2016 *J. Appl. Phys.* **119** 145302
[7] Guerra J A, Zela F D, Tucto K, Montañez L, Töfflinger J A, Winnacker A and Weingärtner R 2016 *J. Phys. D: Appl. Phys.* **49** 375104
[8] Yuan Z, Li D, Wang M, Chen P, Gong D, Wang L and Yang D 2006 *J. Appl. Phys.* **100** 083106
[9] Chang J S, Jhe J H, Yang M S, Shin J H, Kim K J and Moon D W 2006 *Appl. Phys. Lett.* **89** 181909
[10] Garrido B, Pellegrino P, Garcia C, Navarro-Urrios D, Daldosso N, Pavesi L, Gourbilleau F and Rizk R 2006 *Appl. Phys. Lett.* **89** 163103
[11] Heitmann J, Schmidt M, Zacharias M, Timoshenko V Y, Lisachenko M G and Kashkarov P K 2003 *Mater. Sci. Eng.* B **105** 214
[12] Al C A 2007 Nanoparticles de silicium et ion erbium pour lámplification optique *PhD thesis* Université Claude Bernard-Lyon I
[13] Chryssou C E, Kenyon A J, Iwayama T S, Pitt C W and Hole D E 1999 *Appl. Phys. Lett.* **75** 2011
[14] Franzo G, Boninelli S, Pacifici D, Priolo F, Iacona F and Bongiorno C 2003 *Appl. Phys. Lett.* **82** 3871
[15] Gourbilleau F, Levalois M, Dufour C, Vicens J and Rizk R 2004 *J. Appl. Phys.* **95** 3717
[16] Talbot E, Larde R, Pareige P, Khomenkova L, Hijazi K and Gourbilleau F 2013 *Nanoscale Res. Lett.* **8** 39
[17] Hijazi K, Rizk R, Cardin J, Khomenkova L and Gourbilleau F 2009 *J. Appl. Phys.* **106** 024311
[18] Han H S, Seo S Y and Shin J H 2001 *Appl. Phys. Lett.* **79** 4568
[19] Fafin A, Cardin J, Dufour C and Gourbilleau F 2014 *Optic Express* **22** 12296
[20] Lockwood D J and Pavesi L (ed) 2011 Topics in applied physics *Silicon Photonics II* vol 119 (Berlin : Springer) ch 4
[21] Dumont L, Cardin J, Benzo P, Carrada M, Labbé C, Richard A L, Ingram D C, Jadwisienczak W M and Gourbilleau F 2016 *Energy Mater. Sol. Cells* **145** 84
[22] Li R, Yerci S, Kucheyev S O, van Buuren T and Dal Negro L 2011 *Opt. Express* **19** 5379
[23] Marcus M A and Polman A 1991 *J. Non-Cryst. Solids* **136** 260
[24] Adler D L, Jacobson D C, Eaglesham D J, Marcus A M, Benton J L, Poate J M and Citrin P H 1992 *Appl. Phys. Lett.* **61** 2181
[25] An Y T, Labbé C, Cardin J, Morales M and Gourbilleau F 2013 *Adv. Opt. Mater.* **1** 855
[26] Wang B, Wang X J, de Dood M J A, Guo R M, Wang L, Vanhoutte M, Michel J, Kimerling L C and Zhou Z 2012 *J. Phys. D: Appl. Phys.* **45** 165101
[27] Forouhi A R and Bloomer I 1986 *Phys. Rev.* B **34** 7018
[28] Breard D, Gourbilleau F, Belarouci A, Dufour C and Rizk R 2006 *J. Lumin.* **121** 209
[29] Huang L, Hipps K W, Dickinson J T, Mazur U and Wang X D 1997 *Thin Solid Films* **299** 104
[30] Liang C H, Cardin J, Labbé C and Gourbilleau F 2013 *J. Appl. Phys.* **114** 033103
[31] Garrido B, García C, Seo S Y, Pellegrino P, Navarro-Urrios D, Daldosso N, Pavesi L, Gourbilleau F and Rizk R 2007 *Phys. Rev.* B **76** 245308
[32] Karcher R, Ley L and Johnson R L 1984 *Phys. Rev.* B **30** 1896
[33] Dehan E, Tempe-Boyer P, Henda R, Pedroviejo J J and Scheid E 1995 *Thin Solid Films* **266** 14
[34] Barranco A, Mejias J A, Espinos J P, Caballero A, Gonzales-Elipe A R and Yubero F 2001 *J. Vac. Sci. Technol.* A **19** 136
[35] Cova P, Poulin S, Grenier O and Masut R A 2005 *J. Appl. Phys.* **97** 073518
[36] Taylor J A, Lancaster G M and Rabalais J W 1978 *J. Electron Spectrosc. Relat. Phenom.* **13** 435
[37] Zhang P Z, Chen K J, Lin Z W, Tan D M, Dong H P, Li W, Xu J and Huang X F 2016 *Appl. Phys. Lett.* **108** 111103

[38] Delfino M, Fair J A and Salimian S 1992 *Appl. Phys. Lett.* **60** 341
[39] Saliman S and Delfino M 1991 *J. Appl. Phys.* **70** 3970
[40] Hollinger G 1981 *Appl. Surf. Sci.* **8** 318
[41] Sarma D D and Rao C N R 1980 *J. Electron Spectrosc. Relat. Phenom.* **20** 25
[42] Uwamino Y, Ishizuka T and Yamater H 1984 *J. Electron Spectrosc. Relat. Phenom.* **34** 67
[43] Guerra J A, Angulo J R, Gomez S, Llamoza J, Montañez L M, Tejada A, Töfflinger J A, Winnacker A and Weingärtner R 2016 *J. Phys. D: Appl. Phys.* **49** 195102
[44] Kuritsyn D, Kozanecki A, Przybylinska H and Jantsch W 2003 *Appl. Phys. Lett.* **83** 4160
[45] Hijazi K, Khomenkova L, Gourbilleau F, Cardin J and Rizk R 2009 *J. Lumin.* **129** 1886
[46] Salh R, Czarnowki von A, Zamoryanskaya M V, Kolesnikova E V and Fitting H J 2006 *Phys. Status Solidi* a **203** 2049
[47] Savchyn O, Ruhge F R, Kik P G, Todi R M, Coffey K R, Nukala H and Heinrich H 2007 *Phys. Rev.* B **76** 195419
[48] Watanabe K, Tamaoka H, Fujii M, Moriwaki K and Hayashi S 2002 *Physica* E **13** 1038